THE JOURNAL OF PHYSICAL CHEMISTRY Letters

pubs.acs.org/JPCL Letter

Predicted Optimal Bifunctional Electrocatalysts for the Hydrogen Evolution Reaction and the Oxygen Evolution Reaction Using Chalcogenide Heterostructures Based on Machine Learning Analysis of in Silico Quantum Mechanics Based High Throughput Screening

Lei Ge,[+] Hao Yuan,[+] Yuxiang Min, Li Li, Shiqian Chen, Lai Xu,* and William A. Goddard III*

Cite This: *J. Phys. Chem. Lett.* 2020, 11, 869−876 Read Online

ACCESS | Metrics & More | Article Recommendations | Supporting Information

ABSTRACT: Two-dimensional van der Waals heterostructure materials, particularly transition metal dichalcogenides (TMDC), have proved to be excellent photoabsorbers for solar radiation, but performance for such electrocatalysis processes as water splitting to form H_2 and O_2 is not adequate. We propose that dramatically improved performance may be achieved by combining two independent TMDC while optimizing such descriptors as rotational angle, bond length, distance between layers, and the ratio of the bandgaps of two component materials. In this paper we apply the least absolute shrinkage and selection operator (LASSO) process of artificial intelligence incorporating these descriptors together with quantum mechanics (density functional theory) to predict novel structures with predicted superior performance. Our predicted best system is $MoTe_2/WTe_2$ with a rotation of 300°, which is predicted to have an overpotential of 0.03 V for HER and 0.17 V for OER, dramatically improved over current electrocatalysts for water splitting.

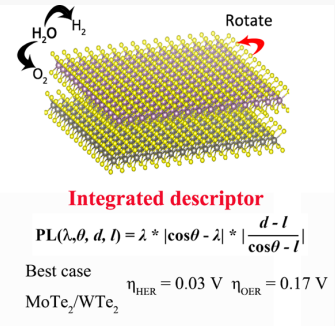

There is an urgent need for clean and efficient sources of reliable energy to accommodate society demands of dramatically improved processes for clean renewable energy. In particular, electrocatalytic water splitting to produce H_2 (and O_2) for use in hydrogen fuel cells to generate power is a most promising future source of energy. Consequently a great amount of research is being dedicated toward electrocatalytic water splitting in which two simultaneous chemical processes occur: the hydrogen evolution reaction (HER) and the oxygen evolution reaction (OER).[1]

Previous experimental and computational studies reported that TMDC can be used in electrocatalytic water splitting. During the past decade, transition metal dichalcogenides (TMDC) have become a most promising 2D material for solar cells, catalysts, and lithium-ion batteries.[2−6] The excellent electrical conductivity and extraordinary catalytic performance of TMDC stem from the ability to effectively transfer electrons, suggesting that they could serve as superior HER cocatalysts.[7] Among the TMDC family, single-layer MX_2 (M = Mo, W; X = S, Se, Te, etc.) are the most studied. They have a direct bandgap,[8] and different MX_2 layers can be stacked to form novel heterojunction materials with deliberately adjusted bandgap.[9] Therefore, we combined these MX_2 monolayers under the condition of low mismatch to investigate their catalytic performance. Previous experimental research reported significant progresses in preparation and synthesis of two-dimensional heterojunctions that could produce high-quality 2D crystal optoelectronic devices.[10,11]

In this study, we consider vertical stacking of van der Waals heterojunction structures of MoS_2/WS_2, $MoSe_2/WSe_2$, MoS_2/WSe_2, $MoSe_2/WS_2$, $MoTe_2/WTe_2$, MoS_2/WTe_2, $MoTe_2/WS_2$, and $MoTe_2/WSe_2$ as candidate bifunctional HER and OER catalysis. We consider the 2H phase structures for all TMDC, although the ground state of WTe_2 is known to be 1T.[12,13] In order to facilitate the comparison of the heterostructures, we chose the 2H phase of the MX_2 to construct the heterostructures.

Doping is commonly used to promote efficient electrocatalysis, but this may destabilize the initial structure. Instead, we propose to optimize the combination of two different TMDC where we also use the relative rotation of these heterostructures to improve electrocatalytic efficiency. Since the interactions between layers are dominated by van der Waals (i.e., or London) forces, we expected that their catalytic performance could be tuned while maintaining the original structure of the TMDC layers. We anticipated that stacking two TMDC layers with specific relative rotational angles might enhance performance. Indeed, Liu et al. put forward a new method to synthesize the 2D moiré superlattice.[14] Their study suggests that the two-dimensional moiré superlattice could

Received: December 29, 2019
Accepted: January 11, 2020
Published: January 11, 2020

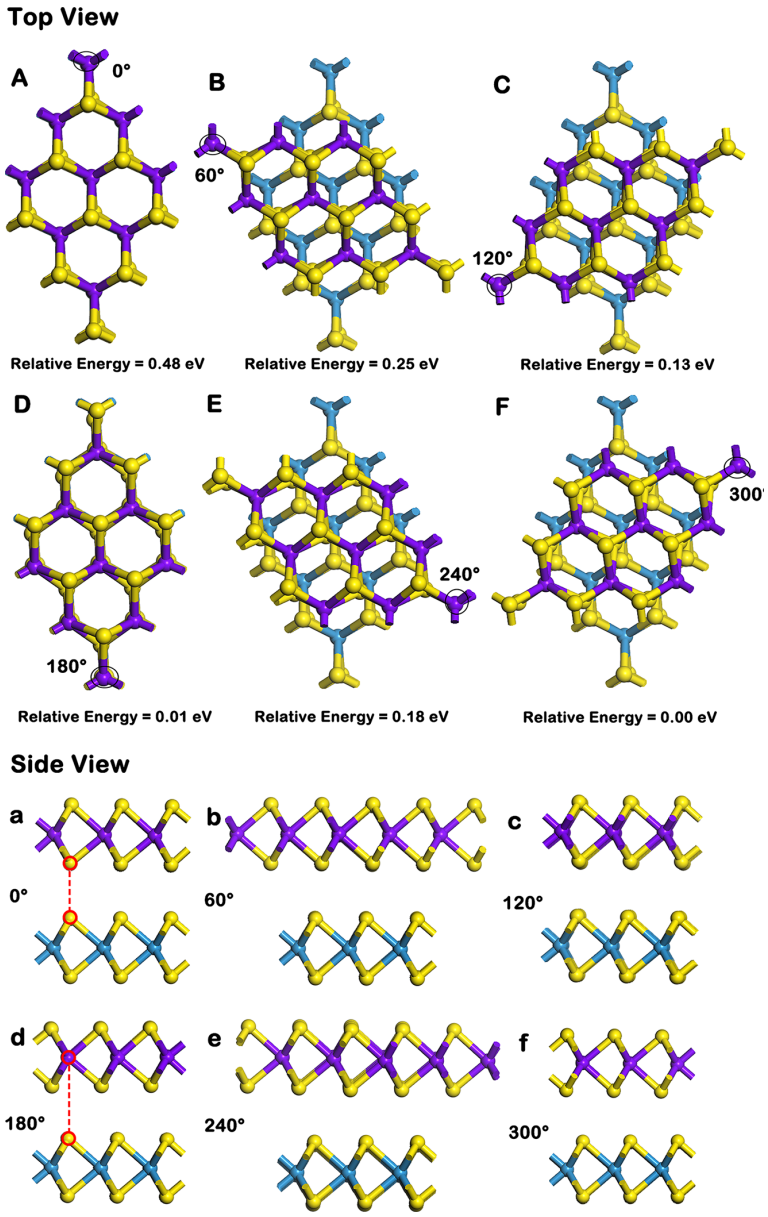

Figure 1. Top view and the side view of the rotation process for the MoS_2/WS_2 heterostructure for (A) 0°, (B) 60°, (C) 120°, (D) 180°, (E) 240°, and (F) 300°, respectively. We list the relative energies with respect to (F) for the optimized structures.

significantly improve the catalytic activity for a wide range of materials. Indeed, several experimental groups[15−17] have applied this method, reporting weak but stable coupling of MX_2 heterostructures with random rotational angles ($0° < \theta < 60°$), which could help stabilize the overall structure. However, stable heterostructures with random relative rotations may not be easy to synthesize due to the large strain and lattice mismatch. For lattice-aligned interfaces, stacking with rotational angles that are multiples of 60° improves stability, making it more likely to be achievable experimentally.[18,19] Therefore, we constructed heterojunctions with relative rotational angles of 0°, 60°, 120°, 180°, 240°, and 300° for all pairs of TMDC to develop a database that we use in our AI analysis.

In order to reduce the computational efforts of using density functional theory (DFT) to develop the data for large numbers of combinations, we used the LASSO (least absolute shrinkage and selection operator) to identify the physical descriptors that significantly affect the adsorption performance.[20−22] By evaluating the error characteristics of predictions for all possible descriptors, we propose the prediction equation for catalytic performance. With the help of machine learning and an optimized algorithm strategy, this saves an enormous amount of time for predicting and modifying structures and performance for new materials, while maintaining high

https://dx.doi.org/10.1021/acs.jpclett.9b03875
J. Phys. Chem. Lett. 2020, 11, 869−876

accuracy and convenience of DFT calculations. Thus, we trained the LASSO regression to extract linear correlations to predict new systems from calculated data. Many descriptors for single atom catalysts and intrinsic catalysts have been proposed, including d-band center,[23,24] generalized coordination number (GCN),[25,26] coordination number (CN),[27] electronegativity,[28] and formation energy.[29] Instead, we consider the rotation angle of TMDC heterojunctions as a descriptor to characterize their catalytic performance. Thus, we used four variables,

- the cosine of the rotational angle θ,
- the distance d between two secondary parts,
- the average bond length l of MX_2,
- and the ratio of the bandgaps of two component materials $E_{g_{rot}}$ and $E_{g_{sub}}$, which is $\frac{E_{g_{rot}}}{E_{g_{sub}}}$ abbreviated as λ,

which we introduce into LASSO to fit the linear regression. We used the LASSO algorithm to combine these separate variables into a large number of possible descriptors through various operations. This leads to a best-fit descriptor expression (1), called the LASSO performance descriptor PL,

$$\mathrm{PL}(\lambda, \theta, d, l) = \lambda|\cos\theta - \lambda|\left|\frac{d-l}{\cos\theta - l}\right| \quad (1)$$

which contains all four variables. Substituting variable values into the descriptor expression, we found that a good linear relationship between the PL descriptor and the calculation results, which is $y = -1.73x + 0.18$ for HER, and $y = 1.04x + 0.6$ for OER. Consequently, we can use $\mathrm{PL}(\lambda, \theta, d, l)$ to predict HER and OER bifunctional catalytic performance of an enormous number of rotated TMDC heterostructures without an enormous number of expensive DFT calculations or cumbersome experiments.

Basic Properties of the Heterostructure Materials. To assess whether selected MX_2 structures are suitable for electrocatalytic hydrogen production, we calculated the band structures of single-layer MoS_2, WS_2, WSe_2, $MoSe_2$, $MoTe_2$, and WTe_2 using the Perdew−Burke−Ernzerhof (PBE) implementation of the generalized gradient approximation (GGA)[30,31] including the D3 empirical London dispersion correction with geometry optimization. The results are shown in Figure S1. Since PBE leads to systematic errors in band gaps, we estimate corrected band gaps using DFT+U methods.[32] This leads to the bandgaps of 1.68, 1.78, 1.32, 1.30, 1.08, and 1.04 eV for single-layer MoS_2, WS_2, $MoSe_2$, WSe_2, $MoTe_2$ and WTe_2, respectively, which are consistent with the bandgaps of 1.68,[33] 1.81,[33] 1.44,[34] 1.25,[35] 1.07,[34] and 1.03 eV[35] reported in previous studies.

Previous studies have reported that MX_2 monolayers have many excellent properties, but their catalytic activities in HER and OER catalysis are not adequate. We found that combining MX_2 layers into a heterojunction allows the electronic properties to be tuned while preserving the exceptional characters of the original structures. Thus, we constructed a series of heterojunction structures with these MX_2 layers. Then, we changed the angle between two MX_2 layers to achieve lattice matching for best electrocatalysis performance.

Binding Energy Analysis for the Heterostructures. It is of great importance to determine the growth order of two different layers for vertically stacked heterostructures, that is, whether it is the $M^AX^A_2/M^BX^B_2$ mode (where catalysis occurs on $M^AX^A_2$) or the $M^BX^B_2/M^AX^A_2$ mode (where catalysis occurs on $M^BX^B_2$). Previous experiments indicate that MoS_2/WS_2 has better catalytic performance for HER than WS_2/MoS_2.[36] Therefore, on the basis of the experiment, we expected that the reactions will occur on the more active Mo layer for vertically stacked heterojunction structures. Indeed, formation of van der Waals heterostructures of $MoTe_2$ on MoS_2 has been confirmed experimentally.[37] After constructing structures and calculating reaction surfaces, we considered rotation of MoS_2 and $MoSe_2$ on both WS_2 and WSe_2, respectively. Optimized geometries of MoS_2/WS_2 with six different rotation angles are shown in Figure 1. Each structure was rotated 60° counterclockwise on the basis of the previous structure, as illustrated by changes in the position of the circled atom Mo in Figure 1. Other systems were prepared following the same method.

For rapid analysis we evaluated the stability of heterojunctions by calculating[38]

$$E_{\mathrm{binding}} = E_{\mathrm{bi}} - E_{\mathrm{monoA}} - E_{\mathrm{monoB}}$$

where E_{bi}, E_{monoA}, and E_{monoB} represent relative energies of heterojunction, layer A and layer B, respectively.

We show in Figure S2a that, as the layer rotates, the binding energy first decreases followed by a slight upward trend with 0° being the highest point. More detailed data are shown in Table S2. Since a more negative binding energy means increased stability, we confirmed the stability of all rotated structures. Figure S2a suggests that the binding energies of the heterojunctions depend on the angle. For each system, the binding energies and the angles follow a curved relationship. When the rotational angle is 180°, the binding energies of most of the systems reach the lowest value. Therefore, the most stable heterojunctions are the ones with a rotational angle of 180°. Since the stability of the heterojunctions depends on the layer spacing, we considered how the distance between layers of the heterojunctions depend on rotational angles, as shown in Figure S2b. From Figure S2a, we discovered that the layer spacing and the rotational angles are strongly correlated. Different optimized heterojunctions have different layer spacings, reflecting different strengths of van der Waals forces. The general trend is that layer spacing decreases with increasing angle and rises after 180°. For example, the initial distance between layers of the $MoTe_2/WTe_2$ system is 3.787 Å. As the rotational angle increases, the layer spacing decreases reaching a minimum of 2.193 Å at 180°. As the rotational angle continues to increase, the interlayer distance increases again, reaching 3.605 Å at 300°, and finally returns to the initial structure. Originally, the upper and lower layers of the heterojunction were combined to obtain interactions between non-metal atoms of each (see Figure 1a); from the side view we see that the S atoms are opposite to the S atoms of the second layer. After rotation by 180°, these two layers have interactions between metal atoms and non-metal atoms (see Figure 1d), the S atoms are opposite to the metal atoms Mo of the other layer, which is relatively stronger. On the basis of the above analysis, we find that the heterojunctions with 180° rotation have the shortest layer distance and the most stable binding energy.

Free Energy Analysis of the Heterostructures. Calculations of HER and OER catalysis were based on the active surface of each system with catalytic performance estimated through reaction free energy of each step $\Delta G = \Delta E + \Delta E_{\mathrm{ZPE}} - T\Delta S$, where ΔE is the adsorption energy, ΔE_{ZPE} is the zero point energy difference, and ΔS is the entropy difference between initial state and adsorbed state.[39] Corresponding data of ΔE_{ZPE}

https://dx.doi.org/10.1021/acs.jpclett.9b03875
J. Phys. Chem. Lett. 2020, 11, 869−876

and ΔS are listed in Table S1. In this calculation, we assume the Tafel mechanism for HER:[40−43]

$$H^+ + e^- + * \rightarrow *H \quad (R1)$$

whereas OER reaction consists of four steps:

$$H_2O(g) + * \rightarrow *OH + H^+ + e^- \quad (R2)$$

$$*OH \rightarrow *O + H^+ + e^- \quad (R3)$$

$$*O + H_2O(g) \rightarrow *OOH + H^+ + e^- \quad (R4)$$

$$*OOH \rightarrow * + O_2 + H^+ + e^- \quad (R5)$$

In this sequence, each oxidation step produces an H^+ and an electron, reducing the energy necessary to yield O_2. Regarding the selection of adsorption sites, we considered metal atom and non-metal atom adsorption sites at the edge and basal plane positions. When the rotational angle is 0°, the free energy of HER of MoS_2/WS_2 is 0.29 eV at the edge site by adding 10 Å vacuum and 0.20 eV at the basal plane site; therefore, we chose the basal plane site as the adsorption site, which is consistent with the results reported by Ali[44] on similar 2H-MoS_2 materials. Moreover, although we constructed the structure in which the H atom is adsorbed at the metal site, we found that it goes to the non-metal site after geometry optimization. Therefore, we took the non-metal site on the basal plane as the reaction site, as shown in Figure 2. Other heterojunctions follow the same adsorption pattern. After optimization of *OH, *O, *OOH, and *H adsorption structures, reaction free energies ΔG_{*OH}, ΔG_{*O}, ΔG_{*OOH}, andΔG_{*H} were calculated. For an ideal HER catalyst, ΔG_{*H} should be near 0 eV, while an ideal OER catalyst would have similar reaction free energies in those four charge transfer steps at zero potential (4.92 eV/4 = 1.23 eV).[45] Following such criteria, we predicted the overpotential of HER (η_{HER}) and OER (η_{OER}) from free energy data listed in Tables S3−S10. This compares the catalytic performance among all systems, where η_{HER} equals $|\Delta G_{*H}|/e$ for HER and η_{OER} is determined by the potential limiting step, as is shown in the formula $\eta_{OER} = \max[\Delta G_1, \Delta G_2, \Delta G_3, \Delta G_4]/e - 1.23$. Here, a smaller η means a lower reaction barrier and better performance of the catalyst, as shown in Figure 3a for HER and Figure 3b for OER. Figures S3−S10 are the free-energy diagrams of the four-step reaction path of OER for each system at zero electrode potential. Corresponding diagrams of HER are also shown in Figures S11−S18.

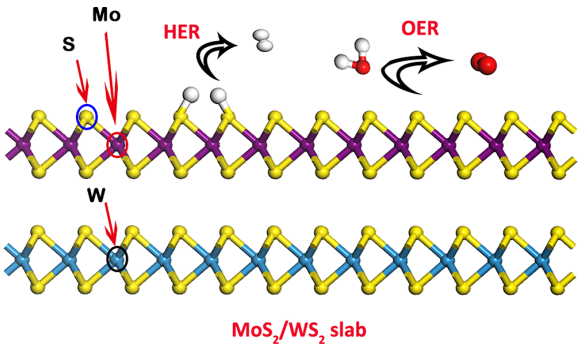

Figure 2. Schematic diagram of the 0°-rotated heterostructure MoS_2/WS_2 configurations for overall water splitting. Purple represents the atom of Mo, yellow represents the atom S, and blue represents the atom W, respectively.

As shown in Figure 3, the MoS_2/WTe_2, $MoTe_2/WS_2$, and $MoTe_2/WSe_2$ systems lead to rather poor electrocatalytic HER performance compared to other systems with overpotentials of HER higher than 1.5 V. This indicates that the heterostructures containing Te have less satisfactory HER performance than MS_2 and MSe_2. In contrast among all systems with overpotential of HER less than 0.5 V, our results show that $MoSe_2/WSe_2$ with a 240° rotation has the small smallest η_{HER} = 0.01 V, making this the best overall candidate for HER (see Figure S12 for details).

For the OER process most cases (MoS_2/WS_2, $MoSe_2/WSe_2$, MoS_2/WSe_2, $MoSe_2/WS_2$, $MoTe_2/WTe_2$, MoS_2/WTe_2, $MoTe_2/WS_2$, and $MoTe_2/WSe_2$) have as the potential-determining step, the third step in which the adsorbed O atom reacts with an H_2O molecule to form the *OOH. However, in the other two systems the final step that generates O_2 determines the rate of the whole reaction process.[46] Overall, $MoTe_2/WTe_2$ with no rotation has the lowest η_{OER} = 0.16 V, whereas 240° rotated $MoSe_2/WSe_2$ are best suited for electrocatalytic HER and 0° $MoTe_2/WTe_2$ are best suited for electrocatalytic OER.

OER is kinetically difficult since it involves the transfer of 4 electrons, usually with a high overpotential. We consider that the ideal catalyst for OER would have a similar energy required for each step instead of a high energy barrier for one step that prevents the reaction from proceeding. As shown in Figure S7, the 0°-rotated $MoTe_2/WTe_2$ structure needs 1.12 eV for an H_2O molecule to decompose on the substrate to generate

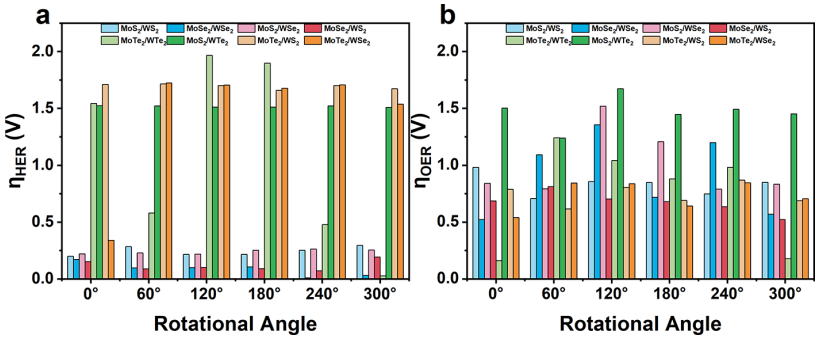

Figure 3. Relationships of the rotational angle with η_{HER} and η_{OER} for each system.

https://dx.doi.org/10.1021/acs.jpclett.9b03875
J. Phys. Chem. Lett. 2020, 11, 869−876

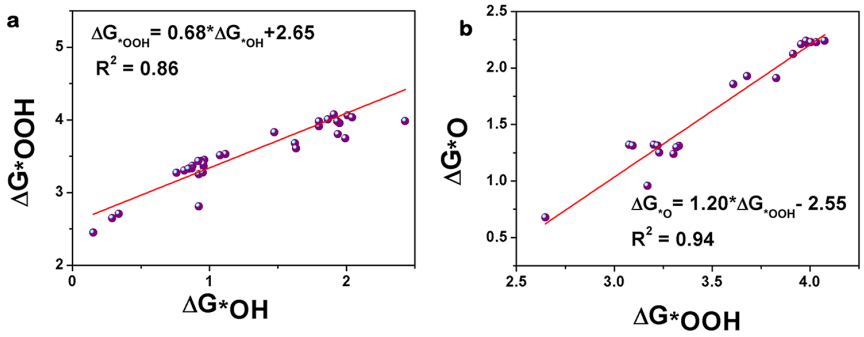

Figure 4. Linear relationships between adsorption free energies: (a) ΔG_{*OOH} and ΔG_{*OH}; (b) ΔG_{*O} and ΔG_{*OOH}.

*OH. Another proton and electron are then lost from *OH to form the *O structure, which requires 1.07 eV. Subsequently, another H_2O molecule reacts with *O to form *OOH. This step requires 1.35 eV energy. The final step, in which *OOH loses a proton and an electron to generate a free oxygen molecule, is the rate-determining step for the whole reaction with the energy change of 1.39 eV. Overall, the energy required in each step is similar, which promotes favorable reaction kinetics.

For HER, we use the Tafel mechanism, which requires the least energy change. For example, as shown in Figure S12, a proton and an electron forms *H on $MoSe_2/WSe_2$. Then, a second H^+ and e^- form a hydrogen molecule, but less energy is required, making the reaction faster. Thus, the 240°-rotated structure performs best for HER. The DFT analysis finds that the $MoTe_2/WTe_2$ system with a rotational angle of 300° exhibits exceptional bifunctional HER (η_{HER} = 0.03 V) and OER (η_{OER} = 0.17 V) catalytic activities for complete water splitting compared to other MX_2 heterojunctions.

As mentioned above, four free energies were calculated for each heterojunction system; hence, a total of 192 data points were obtained from 48 optimized systems. Our initial analysis suggested that there may be a linear correlation between free energies of HER and OER. We studied the relationship of ΔG_{*O}, ΔG_{*OH}, and ΔG_{*OOH}, which we fitted using linear regressions as shown in Figure 4. The relationships are as follows:

$$\Delta G_{*OOH} = 0.68 \times \Delta G_{*OH} + 2.65 \qquad (R^2 = 0.86)$$

$$\Delta G_{*O} = 1.20 \times \Delta G_{*OOH} - 2.55 \qquad (R^2 = 0.94)$$

Root mean squared error (RMSE, R^2) was employed to estimate the prediction performance of the models in this study for linear regression.[47] The best accuracy is achieved between two variables when R^2 approaches 1. From the linear regression equations listed above, we see that the relationships ΔG_{*OOH} is adequate to derive the other free energy changes to describe the correlation between OER catalytic performance for most TMDC systems tested. However, since obtaining ΔG_{*OOH} requires DFT calculations, we want to identify the reactivity of a TMDC system based on inherent properties that could be expressed in terms of a universal descriptor for OER catalysis.

Physical Descriptors Predicted by the LASSO Regression Approach. Our DFT calculations revealed a relationship between the free energy between HER and OER. We used the least absolute shrinkage and selection operator (LASSO)[48−50] in this study, since it automatically finds the most suitable descriptor using the input variables. LASSO is of great help in dealing with this problem giving a linear model with sparse coefficients. By applying a penalty function, LASSO tends to use fewer coefficientsm thereby reducing less relevant dependent variables. Normally, the input parameters for a machine learning model might be the atomic radius, electronegativity, valence electron number, and density of the atoms.[51] Instead, we used structural parameters that greatly influence the heterojunctions including rotational angle ($\cos\theta$) and layer spacing (d) according to their relationship aforementioned, as well as the bond length (l), and the ratio of the bandgaps of two component materials, $E_{g_{rot}}$ and $E_{g_{sub}}$, $\frac{E_{g_{rot}}}{E_{g_{sub}}}$ which is abbreviated to λ, as input parameters. In the descriptor, the distances between layers are the direct and vertical distance between the non-metal atoms of the heterojunction, the bond lengths are the average bond length between the metal and non-metal atoms in the rotated systems, and the band gaps are the top and bottom monolayers of the heterostructure that are available in the online database. Through these descriptors, we used LASSO linear regression to derive a linear equation for supervised learning, effectively predicting the catalytic performance of two-dimensional heterojunction materials of other systems and reducing unnecessary calculations. Combining the parameters affecting the heterojunction structures with the LASSO linear regression, we established a predictive model for screening the superior overpotential for OER performance of heterojunctions. In this calculation, we used five variables as inputs, the ratio of band gaps, rotational angles and their cosine values, distances between layers, and bond length, and we use η_{OER} as the output. Due to the limited size of the data set (48 points), the code for big data analysis was deployed in MATLAB.[29] By modifying the code specifically for this work, we obtained proper descriptors for the linear regression. We found the most suitable descriptor through the following three steps:

Step 1, set up primary variables mentioned above to run a big data code that generates a descriptor set.

Step 2, narrow down the top descriptors for η_{OER} by LASSO.

Step 3, further analyze to find the best descriptor.

In step 1, we generated 257 703 possible descriptors by combining one or more input values through operations including addition, subtraction, multiplication, division, absolute value, square, and square root. From these descriptors, LASSO fitted an equation that best describes the linear relationship. We repeated the procedure 50 times,

https://dx.doi.org/10.1021/acs.jpclett.9b03875
J. Phys. Chem. Lett. 2020, 11, 869−876

standardizing the remaining 90% of the training data each time before the LASSO step. After these treatments, η_{OER} were found to be perfectly fitted by the descriptor

$$PL(\lambda, \theta, d, l) = \lambda|\cos\theta - \lambda|\left|\frac{d-l}{\cos\theta - l}\right| \quad (2)$$

where $\lambda = \frac{E_{g_{rot}}}{E_{g_{sub}}}$. The fitted equation leads to $y = 1.04x + 0.6$, $R^2 = 0.83$ for OER, as shown in Figure 5. This establishes that

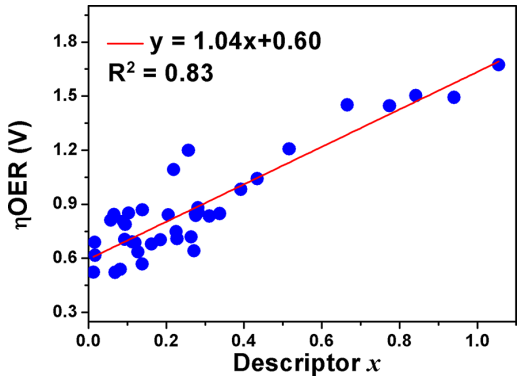

Figure 5. Relationships between the descriptor $PL(\lambda, \theta, d, l) = \lambda|\cos\theta - \lambda|\left|\frac{d-l}{\cos\theta - l}\right|$ and catalytic performance for OER, the relationship between the descriptor x and η_{OER} that was fitted by LASSO regression.

simple combinations of existing intrinsic properties can be found to fit a linear relationship for OER. We found that the linear relationship for HER can be fitted using the same descriptor, leading to $y = -1.73x + 0.18$, $R^2 = 0.80$. Therefore, we conclude that the descriptor $PL(\lambda, \theta, d, l) = \lambda|\cos\theta - \lambda|\left|\frac{d-l}{\cos\theta - l}\right|$ is able to fit the electrocatalytic performance of both HER and OER effectively. Then we used this equation from the LASSO regression to predict the overpotentials of HER and OER. We used the η_{OER} to derive ΔG_{*O}, ΔG_{*OOH}, and ΔG_{*OH}, as shown in Figure 4. The final universal activity descriptor is composed of physical properties obtained from the LASSO regression.

In all, we predicted both HER and OER performance for eight different heterostructures, namely, MoS_2/WS_2, $MoSe_2/WSe_2$, MoS_2/WSe_2, $MoSe_2/WS_2$, $MoTe_2/WTe_2$, MoS_2/WTe_2, $MoTe_2/WS_2$, and $MoTe_2/WSe_2$. We selected vertical stacking structures by comparing bandgaps for various stacking patterns. All heterojunctions constructed here were confirmed to be stable. On the basis of calculating the binding energy of five heterostructures for multiple rotational angles, we found that the most stable structures have a rotational angle of 180°. From reaction free energy analysis of HER and OER catalysis, we discovered that the catalytic performance could be significantly improved by rotating the heterojunction structure. Among all calculated structures, we found that $MoTe_2/WTe_2$ with a rotational angle of 300° has the best overall performance for η_{HER} and η_{OER}, leading to an overpotential of 0.03 V for HER and 0.17 V for OER. These results are better than any current water splitting catalyst.

In order to find the correlation between heterostructures and reaction free energy, we included the following descriptors: rotational angle, bond length, layer distance, and bandgap in the LASSO regression analysis. Through scanning combinations of descriptors using LASSO, we found the best descriptor from the linear regression to be $PL(\lambda, \theta, d, l) = \lambda|\cos\theta - \lambda|\left|\frac{d-l}{\cos\theta - l}\right|$. These results validate our application of LASSO regression of electrocatalytic 2D heterostructure screening catalytic performance of novel TMDC for OER and HER easily without complicated experiments or calculations.

Computational Methods. We carried out spin-polarized density functional theory (DFT) calculations using VASP.[52] We employed the Perdew–Burke–Ernzerhof (PBE) functional[30,31] within the generalized gradient approximation (GGA)[53] to describe the exchange–correlation energy between electrons. We included van der Waals attraction using the DFT-D3 scheme.[30] Interactions between the nuclei and core electrons were described by the projector augmented wave (PAW) method.[54−56] The plane-wave basis set cutoff energy was set at 450 eV. A vacuum slab of 15 Å was set throughout all calculations to avoid interactions between repeated images.

We used a 3 × 3 supercell and 3 × 3 × 1 k-point mesh for all systems. The convergence criteria for energy and force were set to 1.0×10^{-5} eV and −0.05 eV/Å for each atom. GGA+U was set to be 3.4 eV for the d electrons.

For calculations of band structures and density of states (DOS), we employed the Dudarev DFT+U[32] formalism to treat the d states of MoS_2, $MoSe_2$, and $MoTe_2$ and f states of WS_2, WSe_2, and WTe_2, using U values of 3.4 eV to deal with these strongly correlated systems.

The lattice parameters of monolayer MoS_2 and WS_2 are $a = b = 9.498$ Å, of WSe_2 and $MoSe_2$ are $a = b = 9.981$ Å, and of monolayer $MoTe_2$ and WTe_2 are $a = b = 10.67$ Å; thus, their structures are quite similar. A series of heterostructures were built by MX_2 monolayers combining with each other. Adsorbates of *H, *O, *OH, and *OOH were added at the position of the S atom in calculations of adsorption patterns.

■ ASSOCIATED CONTENT

Supporting Information

The Supporting Information is available free of charge at https://pubs.acs.org/doi/10.1021/acs.jpclett.9b03875.

Calculation method of HER and OER activity; structures of heterojunctions; free-energy diagrams for HER and OER of all heterojunctions; tables of binding energies, adsorption free energies, and corrections for gas phase free energies, entropies, and enthalpies (PDF)

■ AUTHOR INFORMATION

Corresponding Authors

Lai Xu − *Institute of Functional Nano & Soft Materials (FUNSOM), Jiangsu Key Laboratory for Carbon-Based Functional Materials & Devices, Soochow University, Suzhou 215123, China;* orcid.org/0000-0003-2473-3359; Email: xulai15@suda.edu.cn

William A. Goddard III − *Materials and Process Simulation Center (MSC) and Joint Center for Artificial Photosynthesis (JCAP), California Institute of Technology, Pasadena, California 91125, United States;* orcid.org/0000-0003-0097-5716; Email: wag@caltech.edu

https://dx.doi.org/10.1021/acs.jpclett.9b03875
J. Phys. Chem. Lett. 2020, 11, 869−876

Other Authors

Lei Ge − *Institute of Functional Nano & Soft Materials (FUNSOM), Jiangsu Key Laboratory for Carbon-Based Functional Materials & Devices, Soochow University, Suzhou 215123, China*

Hao Yuan − *Institute of Functional Nano & Soft Materials (FUNSOM), Jiangsu Key Laboratory for Carbon-Based Functional Materials & Devices, Soochow University, Suzhou 215123, China;* orcid.org/0000-0003-3323-2855

Yuxiang Min − *Institute of Functional Nano & Soft Materials (FUNSOM), Jiangsu Key Laboratory for Carbon-Based Functional Materials & Devices, Soochow University, Suzhou 215123, China*

Li Li − *Institute of Functional Nano & Soft Materials (FUNSOM), Jiangsu Key Laboratory for Carbon-Based Functional Materials & Devices, Soochow University, Suzhou 215123, China;* orcid.org/0000-0001-9260-823X

Shiqian Chen − *Institute of Functional Nano & Soft Materials (FUNSOM), Jiangsu Key Laboratory for Carbon-Based Functional Materials & Devices, Soochow University, Suzhou 215123, China*

Complete contact information is available at: https://pubs.acs.org/10.1021/acs.jpclett.9b03875

Author Contributions

[+]Contributed equally to this work.

Notes

The authors declare no competing financial interest.

■ ACKNOWLEDGMENTS

We acknowledge financial support from National Key R&D Program of China (Grant No. 2017YFB0701600), the National Natural Science Foundation of China (Grant No. 91961120), Caltech-Soochow Multiscale nanoMaterials Genome Center (MnG), Innovative and Entrepreneurial Doctor (World-Famous Universities) in Jiangsu Province, Talent in Demand in the city of Suzhou. This project is also funded by the Collaborative Innovation Center of Suzhou Nano Science & Technology, the Priority Academic Program Development of Jiangsu Higher Education Institutions (PAPD), the 111 Project, and Joint International Research Laboratory of Carbon-Based Functional Materials and Devices. The Caltech studies were supported by the US NSF (CBET-1805022) and the Joint Center for Artificial Photosynthesis, a DOE Energy Innovation Hub, supported through the Office of Science of the U.S. Department of Energy under Award No. DE-SC0004993.

■ REFERENCES

(1) Lv, R. T.; Robinson, J. A.; Schaak, R. E.; Sun, D.; Sun, Y. F.; Mallouk, T. E.; Terrones, M. Transition Metal Dichalcogenides and Beyond: Synthesis, Properties, and Applications of Single- and Few-Layer Nanosheets. *Acc. Chem. Res.* **2015**, *48*, 897−897.

(2) Zhao, J. X.; Chen, Z. F. Single Mo Atom Supported on Defective Boron Nitride Monolayer as an Efficient Electrocatalyst for Nitrogen Fixation: A Computational Study. *J. Am. Chem. Soc.* **2017**, *139*, 12480−12487.

(3) Wang, W. N.; An, W. J.; Ramalingam, B.; Mukherjee, S.; Niedzwiedzki, D. M.; Gangopadhyay, S.; Biswas, P. Size and Structure Matter: Enhanced CO2 Photoreduction Efficiency by Size-Resolved Ultrafine Pt Nanoparticles on TiO2 Single Crystals. *J. Am. Chem. Soc.* **2012**, *134*, 11276−11281.

(4) Liu, J.; Liu, Y.; Liu, N. Y.; Han, Y. Z.; Zhang, X.; Huang, H.; Lifshitz, Y.; Lee, S. T.; Zhong, J.; Kang, Z. H. Metal-Free Efficient Photocatalyst for Stable Visible Water Splitting via a Two-Electron Pathway. *Science* **2015**, *347*, 970−974.

(5) Heersche, H. B.; Jarillo-Herrero, P.; Oostinga, J. B.; Vandersypen, L. M. K.; Morpurgo, A. F. Bipolar Supercurrent in Graphene. *Nature* **2007**, *446*, 56−59.

(6) Profeta, G.; Calandra, M.; Mauri, F. Phonon-Mediated Superconductivity in Graphene by Lithium Deposition. *Nat. Phys.* **2012**, *8*, 131−134.

(7) Zhou, X.; Lin, S.-H.; Yang, X.; Li, H.; Hedhili, M. N.; Li, L.-J.; Zhang, W.; Shi, Y. MoSx-Coated NbS2 Nanoflakes Grown on Glass Carbon: An Advanced Electrocatalyst for the Hydrogen Evolution Reaction. *Nanoscale* **2018**, *10*, 3444−3450.

(8) Shi, Y. M.; Li, H. N.; Li, L. J. Recent Advances in Controlled Synthesis of Two-Dimensional Transition Metal Dichalcogenides via Vapour Deposition Techniques. *Chem. Soc. Rev.* **2015**, *44*, 2744−2756.

(9) Chhowalla, M.; Shin, H. S.; Eda, G.; Li, L. J.; Loh, K. P.; Zhang, H. The Chemistry of Two-Dimensional Layered Transition Metal Dichalcogenide Nanosheets. *Nat. Chem.* **2013**, *5*, 263−275.

(10) Abidi, I. H.; Weng, L.-T.; Wong, C. P. J.; Tyagi, A.; Gan, L.; Ding, Y.; Li, M.; Gao, Z.; Xue, R.; Hossain, M. D.; et al. New Approach to Unveiling Individual Atomic Layers of 2D Materials and Their Heterostructures. *Chem. Mater.* **2018**, *30*, 1718−1728.

(11) Ding, Y.; Peng, Q.; Gan, L.; Wu, R.; Ou, X.; Zhang, Q.; Luo, Z. Stacking-Mode-Induced Reactivity Enhancement for Twisted Bilayer Graphene. *Chem. Mater.* **2016**, *28*, 1034−1039.

(12) Koda, D. S.; Bechstedt, F.; Marques, M.; Teles, L. K. Coincidence Lattices of 2D Crystals: Heterostructure Predictions and Applications. *J. Phys. Chem. C* **2016**, *120*, 10895−10908.

(13) Zhuang, H. L.; Hennig, R. G. Computational Search for Single-Layer Transition-Metal Dichalcogenide Photocatalysts. *J. Phys. Chem. C* **2013**, *117*, 20440−20445.

(14) Liu, L.; Sun, Y.; Cui, X.; Qi, K.; He, X.; Bao, Q.; Ma, W.; Lu, J.; Fang, H.; Zhang, P.; et al. Bottom-up Growth of Homogeneous Moiré Superlattices in Bismuth Oxychloride Spiral Nanosheets. *Nat. Commun.* **2019**, *10*, 4472.

(15) Hong, X. P.; Kim, J.; Shi, S. F.; Zhang, Y.; Jin, C. H.; Sun, Y. H.; Tongay, S.; Wu, J. Q.; Zhang, Y. F.; Wang, F. Ultrafast Charge Transfer in Atomically Thin MoS2/WS2 Heterostructures. *Nat. Nanotechnol.* **2014**, *9*, 682−686.

(16) Ceballos, F.; Bellus, M. Z.; Chiu, H. Y.; Zhao, H. Ultrafast Charge Separation and Indirect Exciton Formation in a MoS2-MoSe2 van Der Waals Heterostructure. *ACS Nano* **2014**, *8*, 12717−12724.

(17) Zhu, H. M.; Wang, J.; Gong, Z. Z.; Kim, Y. D.; Hone, J.; Zhu, X. Y. Interfacial Charge Transfer Circumventing Momentum Mismatch at Two-Dimensional van Der Waals Heterojunctions. *Nano Lett.* **2017**, *17*, 3591−3598.

(18) Wang, H.; Bang, J.; Sun, Y. Y.; Liang, L. B.; West, D.; Meunier, V.; Zhang, S. B. The Role of Collective Motion in the Ultrafast Charge Transfer in van Der Waals Heterostructures. *Nat. Commun.* **2016**, *7*, 11504.

(19) Zhang, J.; Hong, H.; Lian, C.; Ma, W.; Xu, X. Z.; Zhou, X.; Fu, H. X.; Liu, K. H.; Meng, S. Interlayer-State-Coupling Dependent Ultrafast Charge Transfer in MoS2/WS2 Bilayers. *Adv. Sci.* **2017**, *4*, 1700086.

(20) Moraes, L. O.; Pedreira, C. E.; Barrena, S.; Lopez, A.; Orfao, A. A Decision-Tree Approach for the Differential Diagnosis of Chronic Lymphoid Leukemias and Peripheral B-Cell Lymphomas. *Comput. Methods Programs Biomed.* **2019**, *178*, 85−90.

(21) He, Y. Y.; Qin, Y.; Lei, X. H.; Feng, N. P. A Study on Short-Term Power Load Probability Density Forecasting Considering Wind Power Effects. *Int. J. Electr. Power Energy Syst.* **2019**, *113*, 502−514.

(22) Giordano, L.; Baistrocchi, M.; Pacchioni, G. Bonding of Pd, Ag, and Au Atoms on MgO(100) Surfaces and MgO/Mo(100) Ultra-Thin Films: A Comparative DFT Study. *Phys. Rev. B: Condens. Matter Mater. Phys.* **2005**, *72*, 115403.

(23) Hammer, B.; Morikawa, Y.; Norskov, J. K. CO Chemisorption at Metal Surfaces and Overlayers. *Phys. Rev. Lett.* **1996**, *76*, 2141−2144.
(24) Hammer, B.; Norskov, J. K. Theoretical Surface Science and Catalysis - Calculations and Concepts. *Adv. Catal.* **2000**, *45*, 71−129.
(25) Calle-Vallejo, F.; Martinez, J. I.; Garcia-Lastra, J. M.; Sautet, P.; Loffreda, D. Fast Prediction of Adsorption Properties for Platinum Nanocatalysts with Generalized Coordination Numbers. *Angew. Chem., Int. Ed.* **2014**, *53*, 8316−8319.
(26) Calle-Vallejo, F.; Tymoczko, J.; Colic, V.; Vu, Q. H.; Pohl, M. D.; Morgenstern, K.; Loffreda, D.; Sautet, P.; Schuhmann, W.; Bandarenka, A. S. Finding Optimal Surface Sites on Heterogeneous Catalysts by Counting Nearest Neighbors. *Science* **2015**, *350*, 185−189.
(27) Xu, H. X.; Cheng, D. J.; Gao, Y.; Zeng, X. C. Assessment of Catalytic Activities of Gold Nanoclusters with Simple Structure Descriptors. *ACS Catal.* **2018**, *8*, 9702−9710.
(28) Xu, H.; Cheng, D.; Cao, D.; Zeng, X. C. A Universal Principle for a Rational Design of Single-Atom Electrocatalysts. *Nat. Catal.* **2018**, *1*, 339−348.
(29) O'Connor, N. J.; Jonayat, A. S. M.; Janik, M. J.; Senftle, T. P. Interaction Trends between Single Metal Atoms and Oxide Supports Identified with Density Functional Theory and Statistical Learning. *Nat. Catal.* **2018**, *1*, 531−539.
(30) Perdew, J. P.; Burke, K.; Ernzerhof, M. Generalized Gradient Approximation Made Simple. *Phys. Rev. Lett.* **1996**, *77*, 3865−3868.
(31) Perdew, J. P.; Burke, K.; Wang, Y. Generalized Gradient Approximation for the Exchange-Correlation Hole of a Many-Electron System. *Phys. Rev. B: Condens. Matter Mater. Phys.* **1996**, *54*, 16533−16539.
(32) Xu, S.; Carter, E. A. Theoretical Insights into Heterogeneous (Photo)Electrochemical CO2 Reduction. *Chem. Rev.* **2019**, *119*, 6631−6669.
(33) Wei, X. L.; Zhang, H.; Guo, G. C.; Li, X. B.; Lau, W. M.; Liu, L. M. Modulating the Atomic and Electronic Structures through Alloying and Heterostructure of Single-Layer MoS2. *J. Mater. Chem. A* **2014**, *2*, 2101−2109.
(34) Ma, Y.; Dai, Y.; Guo, M.; Niu, C.; Lu, J.; Huang, B. Electronic and Magnetic Properties of Perfect, Vacancy-Doped, and Nonmetal Adsorbed MoSe2, MoTe2 and WS2Monolayers. *Phys. Chem. Chem. Phys.* **2011**, *13*, 15546−15553.
(35) Kang, J.; Tongay, S.; Zhou, J.; Li, J.; Wu, J. Band Offsets and Heterostructures of Two-Dimensional Semiconductors. *Appl. Phys. Lett.* **2013**, *102*, 012111.
(36) Shi, J. P.; Tong, R.; Zhou, X. B.; Gong, Y.; Zhang, Z. P.; Ji, Q. Q.; Zhang, Y.; Fang, Q. Y.; Gu, L.; Wang, X. N.; et al. Temperature-Mediated Selective Growth of MoS2/WS2 and WS2/MoS2 Vertical Stacks on Au Foils for Direct Photocatalytic Applications. *Adv. Mater.* **2016**, *28*, 10664−10672.
(37) Ding, Y.; Zhou, N.; Gan, L.; Yan, X.; Wu, R.; Abidi, I. H.; Waleed, A.; Pan, J.; Ou, X.; Zhang, Q.; et al. Stacking-Mode Confined Growth of 2H-MoTe2/MoS2 Bilayer Heterostructures for UV−Vis−IR Photodetectors. *Nano Energy* **2018**, *49*, 200−208.
(38) Hu, X. H.; Kou, L. Z.; Sun, L. T. Stacking Orders Induced Direct Band Gap in Bilayer MoSe2-WSe2 Lateral Heterostructures. *Sci. Rep.* **2016**, *6*, 31122.
(39) Hinnemann, B.; Moses, P. G.; Bonde, J.; Jorgensen, K. P.; Nielsen, J. H.; Horch, S.; Chorkendorff, I.; Norskov, J. K. Biornimetic Hydrogen Evolution: MoS2 Nanoparticles as Catalyst for Hydrogen Evolution. *J. Am. Chem. Soc.* **2005**, *127*, 5308−5309.
(40) An, Y.-R.; Fan, X.-L.; Luo, Z.-F.; Lau, W.-M. Nanopolygons of Monolayer MS2: Best Morphology and Size for HER Catalysis. *Nano Lett.* **2017**, *17*, 368−376.
(41) Wang, X.; Gan, X.; Hu, T.; Fujisawa, K.; Lei, Y.; Lin, Z.; Xu, B.; Huang, Z.-H.; Kang, F.; Terrones, M.; et al. Noble-Metal-Free Hybrid Membranes for Highly Efficient Hydrogen Evolution. *Adv. Mater.* **2017**, *29*, 1603617.
(42) Zhao, X.; Fu, D.; Ding, Z.; Zhang, Y.-Y.; Wan, D.; Tan, S. J. R.; Chen, Z.; Leng, K.; Dan, J.; Fu, W.; et al. Mo-Terminated Edge Reconstructions in Nanoporous Molybdenum Disulfide Film. *Nano Lett.* **2018**, *18*, 482−490.
(43) Jiang, W.; Zou, X.; Du, H.; Gan, L.; Xu, C.; Kang, F.; Duan, W.; Li, J. Universal Descriptor for Large-Scale Screening of High-Performance MXene-Based Materials for Energy Storage and Conversion. *Chem. Mater.* **2018**, *30*, 2687−2693.
(44) Ali, T.; Wang, X.; Tang, K.; Li, Q.; Sajjad, S.; Khan, S.; Farooqi, S. A.; Yan, C. SnS2 Quantum Dots Growth on MoS2: Atomic-Level Heterostructure for Electrocatalytic Hydrogen Evolution. *Electrochim. Acta* **2019**, *300*, 45−52.
(45) Man, I. C.; Su, H. Y.; Calle-Vallejo, F.; Hansen, H. A.; Martinez, J. I.; Inoglu, N. G.; Kitchin, J.; Jaramillo, T. F.; Norskov, J. K.; Rossmeisl, J. Universality in Oxygen Evolution Electrocatalysis on Oxide Surfaces. *ChemCatChem* **2011**, *3*, 1159−1165.
(46) Yang, L.; Yu, G.; Ai, X.; Yan, W.; Duan, H.; Chen, W.; Li, X.; Wang, T.; Zhang, C.; Huang, X. Efficient Oxygen Evolution Electrocatalysis in Acid by a Perovskite with Face-Sharing IrO 6 Octahedral Dimers. *Nat. Commun.* **2018**, *9*, 5236.
(47) Shahlaei, M.; Madadkar-Sobhani, A.; Fassihi, A.; Saghaie, L.; Arkan, E. QSAR Study of Some CCR5 Antagonists as Anti-HIV Agents Using Radial Basis Function Neural Network and General Regression Neural Network on the Basis of Principal Components. *Med. Chem. Res.* **2012**, *21*, 3246−3262.
(48) Hastie, T.; Friedman, J.; Tibshirani, R. *The Elements of Statistical Learning: Data Mining, Inference, and Prediction*; Springer: New York, NY, 2001.
(49) Ghiringhelli, L. M.; Vybiral, J.; Levchenko, S. V.; Draxl, C.; Scheffler, M. Big Data of Materials Science: Critical Role of the Descriptor. *Phys. Rev. Lett.* **2015**, *114*, 105503.
(50) Ghiringhelli, L. M.; Vybiral, J.; Ahmetcik, E.; Ouyang, R. H.; Levchenko, S. V.; Draxl, C.; Scheffler, M. Learning Physical Descriptors for Materials Science by Compressed Sensing. *New J. Phys.* **2017**, *19*, 023017.
(51) Sun, M. Z.; Wu, T.; Xue, Y. R.; Dougherty, A. W.; Huang, B. L.; Li, Y. L.; Yan, C. H. Mapping of Atomic Catalyst on Graphdiyne. *Nano Energy* **2019**, *62*, 754−763.
(52) Kresse, G.; Furthmuller, J. Efficient Iterative Schemes for Ab Initio Total-Energy Calculations Using a Plane-Wave Basis Set. *Phys. Rev. B: Condens. Matter Mater. Phys.* **1996**, *54*, 11169−11186.
(53) Wu, M. S.; Xu, B.; Liu, G.; Ouyang, C. Y. The effect of strain on band structure of single-layer MoS2: an ab initio study. *Acta Phys. Sin.* **2012**, *61*, 227102.
(54) Goyal, A.; Gorai, P.; Peng, H. W.; Lany, S.; Stevanovic, V. A Computational Framework for Automation of Point Defect Calculations. *Comput. Mater. Sci.* **2017**, *130*, 1−9.
(55) Vanderbilt, D. Soft Self-Consistent Pseudopotentials in a Generalized Eigenvalue Formalism. *Phys. Rev. B: Condens. Matter Mater. Phys.* **1990**, *41*, 7892−7895.
(56) Kresse, G.; Hafner, J. Norm-Conserving and Ultrasoft Pseudopotentials for First-Row and Transition-Elements. *J. Phys.: Condens. Matter* **1994**, *6*, 8245−8257.

https://dx.doi.org/10.1021/acs.jpclett.9b03875
J. Phys. Chem. Lett. 2020, 11, 869−876